Controlled Transport of Particles Using Graphene Patterns

Zhihao Li, Jinfeng Li, Zelin Guo, Jian Xu, and Min Jiang

***Abstract*—We propose the graphene film with trapezoid-shaped nanoparticles (GTNAs) to transport particles. In our design, the conversion of plasmon surface resonances can be realized without changing the excitation light source. By sequentially activating three closely packed potential wells, nanoparticles can be transported between adjacent traps in a creeping manner. Three adjacent potential wells form a linearly repeating array structure, forming a nano-optical conveyor belt. When the resonant wavelength is 5.5 μm, and the power density is 0.4 mW/μm^2, we verified that the target particle can move along the direction of the hot spots. In addition, the movement of nanoparticles in a liquid environment will be interfered with by viscous resistance and the random Brownian motion process. Since particles produce hysteresis or derailment during transmission, we also analyzed the time interval of switching the Fermi level to manipulate the particle in real-time. The three-dimensional finite-difference time-domain method has been used to verify that the design of this paper provides a conveyor belt in tunable graphene without rotating the polarization angle of the light source and has broad application prospects in biomedical diagnostics.**

***Index Terms*—Graphene, metasurfaces, nanoparticle, optical trap, tunable.**

I. Introduction

OPTICAL tweezers (OTs), which focus laser beams tightly, are powerful tools for trapping and manipulating target particles and have wide applications in biological and nanoscience and technology [1]. Conventional OTs usually rely on diffraction to focus the light spot [2] but require very high optical power to generate optical gradient forces, which can generate a large amount of heat and cause sample damage [3]. In addition, traditional diffraction-limited architectures also limit practical applications because it is difficult to position the target particles precisely when trapping them. Plasmonic metasurfaces have been extensively studied in recent decades because they can confine nanoparticles to the most intense hot spots created by metasurface structures. Usually, researchers use two methods to excite the plasmonic metasurfaces to generate highly localized light fields (i.e., the hot spots). One method is to sequentially adjust the incident wavelength of the light source sequentially [4], and the other is to continuously switch the polarization angle of the light source [5], [6], [7]. Jiang et al. proposed a gold plasmonic nano-ellipses array structure that continuously rotates the polarization angle of the light source so that the trapped particles are transported around the edge of the nano-ellipses [8]. Hansen et al. designed a C-aperture array of conveyor belt to transport polystyrene particles by switching different wavelengths [9]. In addition, researchers have proposed various nanostructures designed to generate sufficiently sizeable optical gradient forces at low power, such as nanodisks [10], non-concentric nano-rings [11], gold stripe [12], and nano-antenna [13]. Nevertheless, their fixed structure usually limits the performance of metal plasmonic optical tweezers. This results in the inability to flexibly change optical properties, such as resonant frequencies or the location of local field enhancement during design and experimentation. Furthermore, monitoring and observing nanoparticles is a challenge due to the opaque nature of metal structures.

Using graphene instead of metal materials can solve the above problems because graphene has electrical tunability, efficient thermal conductivity and excellent light transmittance [14], [15]. The carrier density in graphene can be changed by adjusting the gate voltage, thereby affecting the position of the Fermi level and ultimately modulating the local field enhancement factor [16], [17], [18]. In the past decade, researchers have proposed various graphene plasmonic metasurface structures, such as rings [19], [20], [21], disks [22], [23], [24], ribbons [25], [26], [27], and so on [28], [29], [30], [31]. Liu et al. designed a two-dimensional conveyor belt network of graphene metasurfaces that can trap many particles and transport them independently to any target area [32]. Khorami et al. presented a lab-on-a-chip tweezer device based on an isosceles-triangle-shaped graphene nano-taper that can trap sub-wavelength nanoparticles [33]. Kim et al. proposed nanohole to trap target particles [34]. Comparing graphene nanoholes with gold nanoholes proves that graphene nanoholes have more substantial trapping power and verifies that graphene has an advantage in generating minimal heat.

Here, we report a plasmonic metasurface optical conveyor belt with tunable functionality. It is constructed from a pair of graphene trapezoid-shaped nanoapertures (GTNAs). Its working principle and particle transmission characteristics are analyzed by controlling the local field enhancement by adjusting the back-gate voltage at the appropriate incident wavelength. Polystyrene nanoparticle (PS-NP) will move along the hot spots

Manuscript received 1 March 2024; revised 12 April 2024; accepted 19 April 2024. Date of publication 23 April 2024; date of current version 2 May 2024. This work was supported by the National Natural Science Foundation of China (NSFC) under Grant 62105161. *(Corresponding author: Min Jiang.)*

Zhihao Li, Jinfeng Li, Zelin Guo, and Jian Xu are with the School of Automation, Nanjing University of Information Science and Technology, Nanjing 210044, China (e-mail: 202212490509@nuist.edu.cn; 202212490511@nuist.edu.cn; 20211249564@nuist.edu.cn; 1936353611@qq.com).

Min Jiang is with the Faculty of Science, Wuxi University, Wuxi 214105, China (e-mail: 880154@cwxu.edu.cn).

Digital Object Identifier 10.1109/JPHOT.2024.3392641

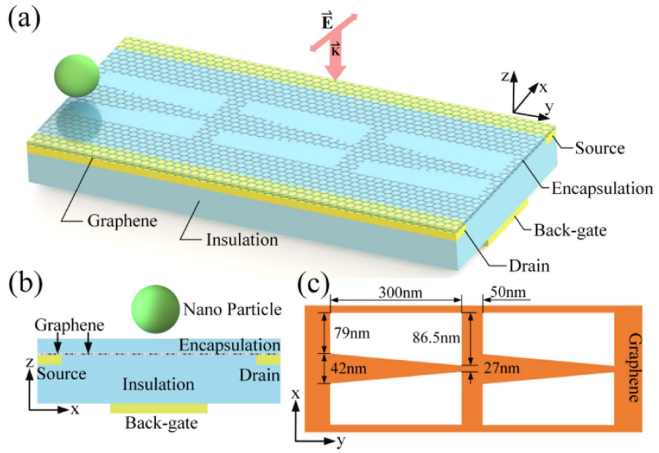

Fig. 1. Schematic illustration of (a) a three-dimensional view and (b) a view of the cross-section of GTNAs. (c) The parameters of GTNAs.

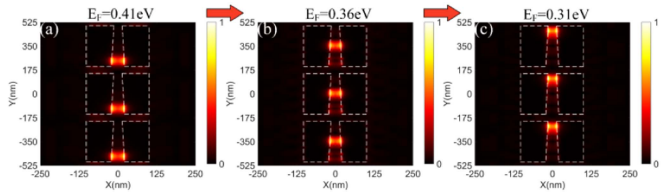

Fig. 2. (a), (b), and (c) are two-dimensional schematics of the normalized electric field intensity distribution on the GTNAs and 10 nm above the surface, respectively.

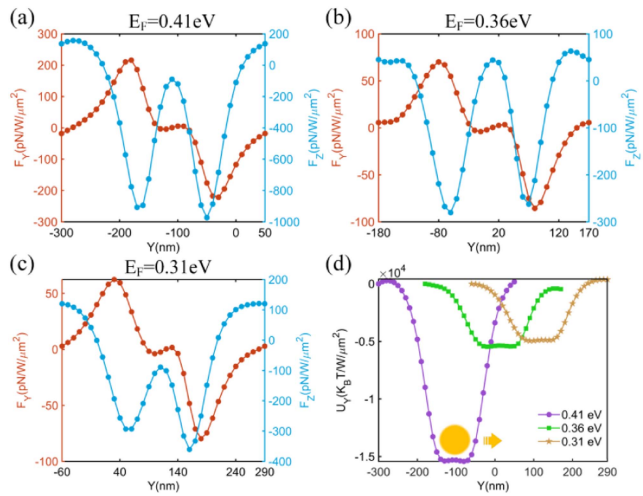

Fig. 3. (a) Forces on particles passing through GTNAs with the Fermi level of 0.41 eV. (b) with the Fermi level of 0.36 eV. (c) with the Fermi level of 0.31 eV. (d) The distribution of the potential well with different Fermi levels.

path due to the tightly packed local field gradient force provided by graphene. The optical gradient force field distribution is analyzed using the three-dimensional finite-difference time-domain (FDTD) method, and the Volumetric Technique is used to measure the force on the trapped target. The modeling results fully support the feasibility of our design. On this basis, simulation and statistical analysis were conducted on the motion distribution of particles in a liquid solution environment under different Fermi level switching intervals. Undoubtedly, this has broad application prospects in the medical field.

II. Graphene Metasurface Design and Method

Fig. 1(a) shows that a graphene plasmonic metasurface consists of a pair of trapezoidal nanoapertures symmetrical about the Y-axis, arranged sequentially to form a periodic array structure. The GTNAs are encapsulated between a silicon dioxide substrate and a dielectric layer to protect GTNAs from the liquid environment. The thickness of substrate and dielectric layer is 200 nm and 5 nm, respectively. Fig. 1(b) shows the application of an external voltage on the metal back-gate at the bottom of the structure to change the Fermi level of graphene and cause it to excite resonance. The structural device is wholly placed in water, with the particle having a diameter of 400 nm and located 10 nm above the graphene film. Fig. 1(c) shows the structural dimensions of graphene as follows. The base length of the nanoaperture is 300 nm, the heights on both sides are 79 nm and 86.5 nm, respectively, and the intervals between a pair of symmetrical nanoapertures are 42 nm and 27 nm, respectively. The pair of nanoapertures are periodically arranged on the Y-axis, with a 50 nm interval between each pair.

Fig. 2 shows the two-dimensional local field intensity distribution of the GTNA structure. The incident light is an X-axis polarized plane wave of 5.5 μm, and the light source is irradiated from top to bottom perpendicular to the Z-axis. The Fermi level of graphene is adjusted to 0.41 eV, 0.36 eV, and 0.31 eV in sequence, and the plasmonic metasurface excites resonance at two symmetrical GTNA gaps, forming a transmission channel with three hot spot areas. At a given resonance wavelength, the intensity of the hot spots depends on the Fermi level and the width of the transmission channel gap. We extensively debugged the structure and selected an optimal gap width to reduce crosstalk between adjacent structures and create an effective hot spot area. As the Fermi level decreases, the hot spots change continuously, guiding the particles forward in the transmission channel.

We calculate the optical gradient force experienced by the particle to discuss the reliability of the design. When the Fermi level $E_F = 0.41$ eV, GTNAs resonate in the lower part (first region) of a transmission period, as shown in Fig. 3(a). The horizontal optical gradient force F_Y and vertical optical gradient force F_Z of the PS-NP are calculated through the volumetric technique, where the target particle material is polystyrene, and the refractive index is 1.59. Fig. 3(b)–(c) shows the components of the optical force exerted by the incident light on the particle in the Y and Z directions when the Fermi level is $E_F = 0.36$ eV and $E_F = 0.31$ eV, respectively. It is worth noting that the horizontal force F_Y changes significantly on the resonance GTNAs. F_Y at zero indicates that the PS-NP will be trapped in the resonance area because there is a robust localization of the field. On the other hand, a negative value for the vertical force F_Z means that the target is dragged above the surface of the GTNAs.

Integrating F_Y along the Y direction can calculate the potential well U_Y. As shown in the golden star line segment in Fig. 3(d), the hot spots intensity at the narrowest position of GTANs has a small excitation efficiency. Under the irradiation of the incident power of 1 W/μm^2, its potential well is about

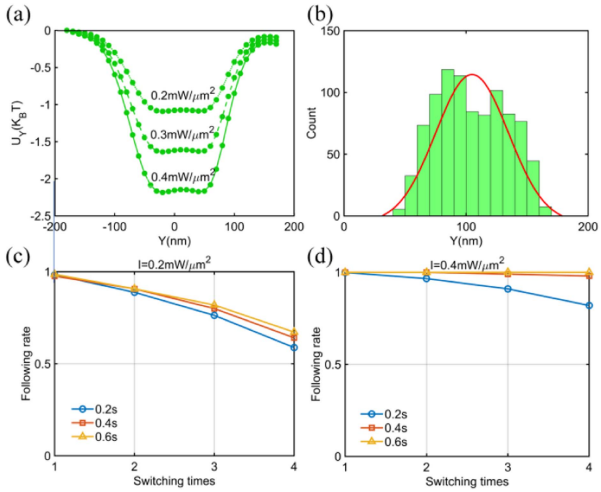

Fig. 4. (a) The potential well depth under different incident light power. (b) Comparison between numerical simulation (green histogram) and theoretical steady-state distribution (red line). When I is set as (c) 0.2 mW/μm^2 and (d) 0.4 mW/μm^2, the function of the following rate and switching times when switching interval (ΔT) is 0.2 s (blue circles), 0.4 s (orange squares), and 0.6 s (yellow triangles).

5000 K_BT, equivalent to 0.2 mW/μm^2 power required for a 1 K_BT potential well. In addition, many GNTAs are periodically arranged to form a channel with long-distance transmission capability, allowing target particles to be transmitted backward.

III. Particle Transport

We used statistical methods to calculate the effects of Brownian motion and viscous resistance of 1000 PS-NPs to simulate the actual scene of the particle transport process. According to Einstein's Brownian motion theory, the random disturbance, diffusion, and force behavior of nanoparticles in liquids are predicted, thereby optimizing the design and operation of OTs. Fig. 4(a) shows that the potential well depth becomes more profound with the increased incident light intensity. We also calculate the distribution of 1000 nanoparticles at an optical power of 0.4 mW/μm^2. As shown in Fig. 4(b), the actual distribution of these particles roughly presents a Gaussian distribution, which is no different from the theoretical curve.

The following rate refers to the total number of particles that can be effectively transmitted to a specified location as a percentage of the total number. When the incident optical power is fixed at 0.2 mW/μm^2, the transport effect of particles through one transmission period was tested. A single transmission period is the time (ΔT) for three switching hot spots, as shown in Fig. 4(c). However, as the number of switches increases, particles following rate decrease significantly because the incident light power is too weak to provide sufficient optical gradient force, and particles cannot be wholly attracted to the next adjacent potential well during transmission. Therefore, Fig. 4(d) shows increasing the power to 0.4 mW/μm^2 to test the relationship between the switching interval and the following rate. When the switching interval is 0.2 s, the following rate drops significantly after four intervals, while 0.4 s and 0.6 s can effectively maintain the following rate above 95%. In order to transport particles more quickly and efficiently, the final switching interval of the Fermi level is set to 0.6 s.

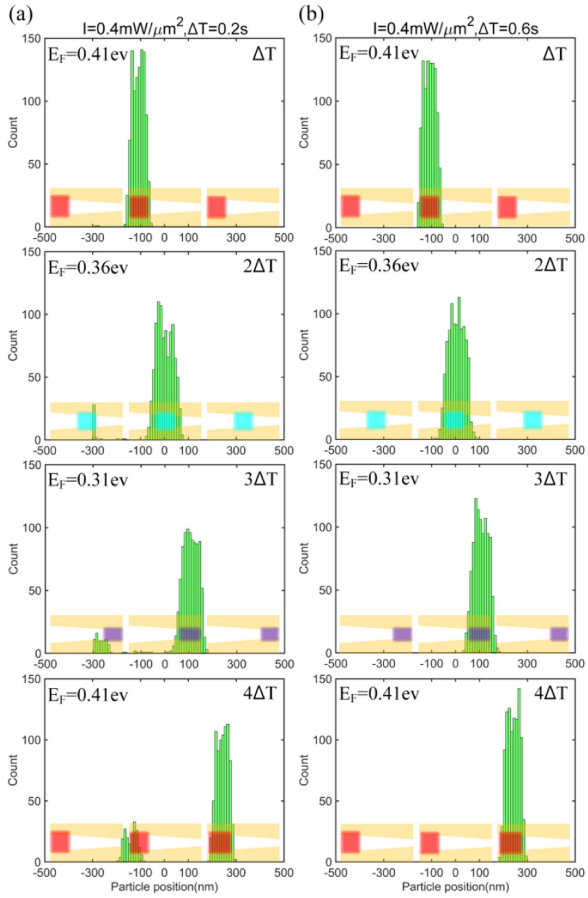

Fig. 5. Particle distribution and transportation at intervals of switching Fermi levels when I is 0.4 mW/μm^2. (a) with a switching interval of 0.2 s, (b) with a switching interval of 0.6 s.

When the time interval for a single switching of the Fermi level is 0.2 s, the position distribution of 1000 particles observed within one transmission period is shown in Fig. 5(a). We found that the particles could not all follow, and some gradually dispersed; this echoes the increasingly lower following rate shown in Fig. 4(c). This situation is because when the switching interval is too short and the number of switches is increasing, some particles cannot follow up in time before the current hot spot disappears, causing them to be pulled to the left of the potential well, so these particles always lag behind the moving potential well even derail. In contrast, Fig. 5(b) shows that setting the switching interval to 0.6 s can ensure that the nanoparticles move toward the expected position and that the following rate is nearly 100%. Among them, the yellow trapezoidal nanoapertures in the background of Fig. 5 represent graphene, the white gaps between graphene are transmission channels, and the colored squares represent hot spots generated by graphene resonance.

Practical applications require lower power because too high a power will cause thermal effects, and the stability of the optical system will also decrease. Therefore, we used the abovementioned lower optical power of 0.4 mW/μm^2 and switching interval of 0.6 s to obtain the particle position distribution of 100 transmission periods. Fig. 6(a) shows that given

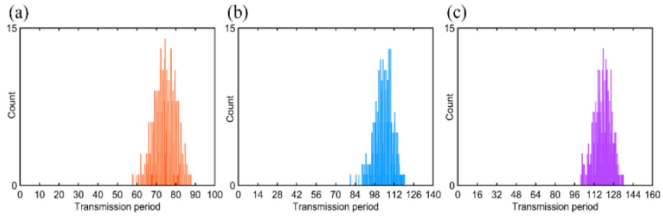

Fig. 6. Particle distributions when (a) 100 transmission periods, (b) 140 transmission periods, and 160 transmission periods have been experienced when I is 0.4 mW/μm^2.

100 transmission periods, most particles are mainly concentrated at 70-80 transmission periods and, therefore, require extra time to reach the designated location. If 40 additional transmission periods are added, 85% of the particles can be effectively transported, as shown in Fig. 6(b). Fig. 6(c) shows that for a specified 100 transmission period, 160 transmission periods are needed to transmit all particles. Therefore, these features are also optional for relatively low-time requirements scenarios.

IV. Conclusion

In conclusion, we proposed a graphene film metasurface structure with trapezoid-shaped nanoapertures to form a transmission channel for transporting polystyrene particles over long distances. The GTNAs structure is mirror symmetric along the Y-axis, and by periodically changing the Fermi level, we can trap and transport nanoparticles in a one-way forward transfer step. At the same time, based on Brownian motion analysis, the conditions for stable particles following under different incident light powers are given, confirming that this design can ensure stable transmission of particles at lower incident light power. Finally, we also demonstrate the ability of this design to transport particles over long distances. Our investigations have broad application prospects in the field of biomedical diagnostics.

Acknowledgment

Data underlying the results presented in this paper are not publicly available at this time but may be obtained from the authors upon reasonable request.

References

[1] D. G. Grier, "A revolution in optical manipulation," *Nature*, vol. 424, no. 6950, pp. 810–816, Aug. 2003.
[2] D. G. Kotsifaki and S. N. Chormaic, "Plasmonic optical tweezers based on nanostructures: Fundamentals, advances and prospects," *Nanophotonics*, vol. 8, no. 7, pp. 1227–1245, 2019.
[3] T. T. Perkins, "Optical traps for single molecule biophysics: A primer," *Laser Photon. Rev.*, vol. 3, no. 1/2, pp. 203–220, 2009.
[4] G. Wang, Z. Ying, H.-P. Ho, Y. Huang, N. Zou, and X. J. O. l. Zhang, "Nano-optical conveyor belt with waveguide-coupled excitation," *Opt. Lett.*, vol. 41, no. 3, pp. 528–531, 2016.
[5] M. Jiang et al., "Integrated optofluidic micro-pumps in micro-channels with uniform excitation of a polarization rotating beam," *Opt. Lett.*, vol. 44, no. 1, pp. 53–56, 2019.
[6] C. Zhang et al., "Optical conveyor belt based on a plasmonic metasurface with polarization dependent hot spot arrays," *Opt. Lett.*, vol. 46, no. 7, pp. 1522–1525, Apr. 2021.
[7] F. Xu et al., "Optically levitated conveyor belt based on polarization-dependent metasurface lens arrays," *Opt. Lett.*, vol. 47, no. 9, pp. 2194–2197, May 2022.
[8] M. Jiang et al., "Two-dimensional arbitrary nano-manipulation on a plasmonic metasurface," *Opt. Lett.*, vol. 43, no. 7, pp. 1602–1605, Apr. 2018.
[9] P. Hansen, Y. Zheng, J. Ryan, and L. Hesselink, "Nano-optical conveyor belt, part I: Theory," *Nano Lett.*, vol. 14, no. 6, pp. 2965–2970, Jun. 2014.
[10] Z. Kang, H. Lu, J. Chen, K. Chen, F. Xu, and H. P. Ho, "Plasmonic graded nano-disks as nano-optical conveyor belt," *Opt. Exp.*, vol. 22, no. 16, pp. 19567–19572, Aug. 2014.
[11] M. Jiang et al., "Plasmonic non-concentric nanorings array as an unidirectional nano-optical conveyor belt actuated by polarization rotation," *Opt. Lett.*, vol. 42, no. 2, pp. 259–262, Jan. 2017.
[12] K. Wang, E. Schonbrun, P. Steinvurzel, and K. B. Crozier, "Scannable plasmonic trapping using a gold stripe," *Nano Lett.*, vol. 10, no. 9, pp. 3506–3511, Sep. 2010.
[13] W. Zhang, L. Huang, C. Santschi, and O. J. Martin, "Trapping and sensing 10 nm metal nanoparticles using plasmonic dipole antennas," *Nano Lett.*, vol. 10, no. 3, pp. 1006–1011, Mar. 2010.
[14] F. J. García de Abajo, "Graphene plasmonics: Challenges and opportunities," *ACS Photon.*, vol. 1, no. 3, pp. 135–152, 2014.
[15] R. R. Nair et al., "Fine structure constant defines visual transparency of graphene," *Science*, vol. 320, no. 5881, pp. 1308–1308, 2008.
[16] T. Low and P. J. A. Avouris, "Graphene plasmonics for terahertz to mid-infrared applications," *ACS Nano*, vol. 8, no. 2, pp. 1086–1101, 2014.
[17] C. Zhou et al., "Tunable Fano resonator using multilayer graphene in the near-infrared region," *Appl. Phys. Lett.*, vol. 112, no. 10, 2018, Art. no. 101904.
[18] L. Ju et al., "Graphene plasmonics for tunable terahertz metamaterials," *Nature Nanotechnol.*, vol. 6, no. 10, pp. 630–634, 2011.
[19] M. Jiang, Z. Guo, H. Li, X. Liu, F. Xu, and G. Wang, "Optical Conveyor Belt With Electrically Tunable Graphene Plasmonic Nanorings," *IEEE Photon. Technol. Lett.*, vol. 35, no. 10, pp. 549–552, May 2023.
[20] Y. Qi et al., "A tunable terahertz metamaterial absorber composed of elliptical ring graphene arrays with refractive index sensing application," *Results Phys.*, vol. 16, 2020, Art. no. 103012.
[21] C. Cen et al., "A dual-band metamaterial absorber for graphene surface plasmon resonance at terahertz frequency," *Physica E: Low-Dimensional Syst. Nanostructures*, vol. 117, 2020, Art. no. 113840.
[22] J. Zhang, Z. Zhu, W. Liu, X. Yuan, and S. J. N. Qin, "Towards photodetection with high efficiency and tunable spectral selectivity: Graphene plasmonics for light trapping and absorption engineering," *Nanoscale*, vol. 7, no. 32, pp. 13530–13536, 2015.
[23] M. Fan, Y. Zhang, D. Chen, L. Ren, Q. Yang, and C. Zhou, "Tunable light trapping in the graphene metasurface," *Appl. Opt.*, vol. 61, no. 36, pp. 10694–10699, Dec. 2022.
[24] Z. Fang et al., "Active tunable absorption enhancement with graphene nanodisk arrays," *Nano Lett.*, vol. 14, no. 1, pp. 299–304, 2014.
[25] V. W. Brar, M. S. Jang, M. Sherrott, J. J. Lopez, and H. A. Atwater, "Highly confined tunable mid-infrared plasmonics in graphene nanoresonators," *Nano Lett.*, vol. 13, no. 6, pp. 2541–2547, 2013.
[26] Z. H. Zhu et al., "Electrically tunable polarizer based on anisotropic absorption of graphene ribbons," *Appl. Phys. A*, vol. 114, no. 4, pp. 1017–1021, 2014.
[27] H. Li, C. Ji, Y. Ren, J. Hu, M. Qin, and L. J. C. Wang, "Investigation of multiband plasmonic metamaterial perfect absorbers based on graphene ribbons by the phase-coupled method," *Carbon*, vol. 141, pp. 481–487, 2019.
[28] J. Chen et al., "Optical nano-imaging of gate-tunable graphene plasmons," *Nature*, vol. 487, no. 7405, pp. 77–81, Jul. 2012.
[29] A. A. Saleh and J. A. Dionne, "Toward efficient optical trapping of sub-10-nm particles with coaxial plasmonic apertures," *Nano Lett.*, vol. 12, no. 11, pp. 5581–5586, Nov. 2012.
[30] B. Xiao, Y. Wang, S. Tong, J. Qin, D. Zhang, and L. Xiao, "Graphene electromagnetically induced transparent polarization-insensitive sensors in the mid-infrared frequency band," *Appl. Opt.*, vol. 62, no. 30, pp. 8178–8183, Oct. 2023.
[31] Z. Fang et al., "Gated tunability and hybridization of localized plasmons in nanostructured graphene," *ACS Nano*, vol. 7, no. 3, pp. 2388–2395, Mar. 2013.
[32] P. Q. Liu and P. Paul, "Graphene nanoribbon plasmonic conveyor belt network for optical trapping and transportation of nanoparticles," *ACS Photon.*, vol. 7, no. 12, pp. 3456–3466, 2020.
[33] A. A. Khorami, B. Barahimi, S. Vatani, and A. S. Javanmard, "Tunable plasmonic tweezers based on graphene nano-taper for nano-bio-particles manipulation: Numerical study," *Opt. Exp.*, vol. 31, no. 13, pp. 21063–21077, Jun. 2023.
[34] J.-D. Kim and Y.-G. Lee, "Graphene-based plasmonic tweezers," *Carbon*, vol. 103, pp. 281–290, 2016.